First normal stress difference and crystallization in a dense sheared granular fluid

Meheboob Alam, and Stefan Luding

View Online

Export Citation

ARTICLES YOU MAY BE INTERESTED IN

Shear thickening, frictionless and frictional rheologies in non-Brownian suspensions
Journal of Rheology **58**, 1693 (2014); https://doi.org/10.1122/1.4890747

Viscosity, granular-temperature, and stress calculations for shearing assemblies of inelastic, frictional disks
Journal of Rheology **30**, 949 (1986); https://doi.org/10.1122/1.549893

Modified kinetic theory applied to the shear flows of granular materials
Physics of Fluids **29**, 043302 (2017); https://doi.org/10.1063/1.4979632

First normal stress difference and crystallization in a dense sheared granular fluid

Meheboob Alam[a)]
Institut für Computeranwendungen 1, Universität Stuttgart, Pfaffenwaldring 27, 70569 Stuttgart, Germany

Stefan Luding
Institut für Computeranwendungen 1, Universität Stuttgart, Pfaffenwaldring 27, 70569 Stuttgart, Germany and Particle Technology, DelftChemTech, TU-Delft, Julianalaan 136, 2628 BL Delft, The Netherlands

The first normal stress difference ($\mathcal{N}_1$) and the microstructure in a dense sheared granular fluid of smooth inelastic hard-disks are probed using event-driven simulations. While the anisotropy in the second moment of fluctuation velocity, which is a Burnett-order effect, is known to be the progenitor of normal stress differences in *dilute* granular fluids, we show here that the collisional anisotropies are responsible for the normal stress behavior in the *dense* limit. As in the elastic hard-sphere fluids, $\mathcal{N}_1$ remains *positive* (if the stress is defined in the *compressive* sense) for dilute and moderately dense flows, but becomes *negative* above a critical density, depending on the restitution coefficient. This sign-reversal of $\mathcal{N}_1$ occurs due to the *microstructural* reorganization of the particles, which can be correlated with a preferred value of the *average* collision angle $\theta_{av} = \pi/4 \pm \pi/2$ in the direction opposing the shear. We also report on the shear-induced *crystal*-formation, signaling the onset of fluid–solid coexistence in dense granular fluids. Different approaches to take into account the normal stress differences are discussed in the framework of the relaxation-type rheological models. © *2003 American Institute of Physics.* [DOI: 10.1063/1.1587723]

I. INTRODUCTION

In the last decade, a lot of research activity took place to unveil the properties of granular materials,[1,2] primarily because of their industrial importance, but also due to their fascinating properties. This has unraveled many interesting and so far unresolved phenomena (for example, clustering, size-segregation, avalanches, the coexistence of gas, liquid and solid, etc.). Under highly excited conditions, granular materials behave as a fluid, with prominent *non-Newtonian* properties, like the normal stress differences.[3] While the normal stress differences are of *infinitesimal* magnitudes in a simple fluid (e.g., air and water), they can be of the order of its isotropic pressure in a dilute granular gas.[4] From the modeling viewpoint, the presence of such large normal-stress differences readily calls for higher-order constitutive models[5,6] even at the *minimal* level.

Studying the non-Newtonian behavior is itself an important issue, since the normal stresses are known to be the *progenitors* of many interesting and unique flow-features (e.g., rod-climbing or Weissenberg-effect, die-swelling, secondary flows, etc.[7]) in non-Newtonian fluids. Also, normal stresses can support additional instability modes (for example, in polymeric fluids and suspensions[7–10]) which might, in turn, explain some flow-features of granular fluids. For example, particle-clustering[11–13] has recently been explained

from the instability-viewpoint using the standard Newtonian model for the stress tensor.[12,14,15]

The kinetic theory of Jenkins and Richman[16] first showed that the *anisotropy* in the second moment of the fluctuation velocities, due to the inelasticity of particle collisions, is responsible for such normal stress behavior. They predicted that the first normal stress difference [defined as $\mathcal{N}_1 = (\Pi_{xx} - \Pi_{yy})/p$, where Π_{xx} and Π_{yy} are the streamwise and the transverse components of the stress deviator, respectively, and p is the isotropic pressure; see Sec. II B] is maximum in the dilute limit, decreases in magnitude with density, and eventually approaches zero in the dense limit. Goldhirsch and Sela[4] later showed that the normal stress differences appear only at the Burnett-order-description of the Chapman–Enskog expansion of the Boltzmann equation. Their work has clearly established that the *origin* of this effect (in the dilute limit) is *universal* in both atomic and granular fluids, with inelasticity playing the role of a *magnifier* and thus making it a sizable effect in granular fluids. While the *source* of the normal stress differences in the dilute limit has been elucidated both theoretically and by simulation, its *dense* counterpart has not received similar attention so far. This is an important limit since the *onset* of *dilatancy* (volume expansion due to shear[17,18]), crystallization, etc., occur in the dense regime, which in turn would influence the normal stress differences.

Previous hard-sphere simulations[3,11,19] did look at the normal stress differences, but they did not probe the *dense* limit in a systematic way. These simulations showed that the first normal stress difference vanishes in the dense limit, in

[a)]Present address: Engineering Mechanics Unit, JNCASR, Bangalore 560064, India. Electronic mail: meheboob@jncasr.ac.in

line with the theoretical predictions of Jenkins and Richman.[16] On the other hand, the soft-sphere simulations of Walton and Braun,[20] with frictional particles, showed that this quantity can change sign in the same limit. Our work with smooth inelastic hard-disks unequivocally demonstrates that $\mathcal{N}_1$, indeed, changes its sign at some critical density in the dense regime, due to the sign-change of its collisional component at a critical density, which depends on the value of the coefficient of restitution (e). More importantly, we show that the origin of $\mathcal{N}_1$ in the dense limit is distinctly different from that in a dilute granular gas. At the *microstructural*-level, certain topological changes in the *anisotropic* structure of the collision-angle distribution with density are responsible for the observed sign-reversal of $\mathcal{N}_1$.

We use the familiar smooth hard-disk model for an event-driven simulation[21] of the uniform shear flow configuration, focusing mainly on the normal stress behavior and the microstructure formation as functions of the density and inelasticity. The details of the simulation technique and the relevant macroscopic quantities are described in Sec. II. The simulation results on the first normal stress difference, the radial distribution function, the collision angle distribution and the crystalline-structure are presented in Sec. III. Possible modeling approaches to incorporate the normal stress differences are discussed in Sec. IV. In Sec. V we summarize our findings, with suggestions for possible future work.

II. SIMULATION METHOD

We consider a collection of smooth inelastic hard-disks in a square box of size $\widetilde{L}$ under uniform shear flow—let $\widetilde{x}$ and $\widetilde{y}$ be the streamwise and transverse directions, respectively, with the origin of the coordinate-frame being positioned at the center of the box. The snapshot of a typical simulation, with nondimensional coordinates, is shown in Fig. 1(a). Note that the dimensional quantities are denoted by overtildes, and the reference length, time and velocity scales for nondimensionalization will be specified later in this section.

Let the diameter and the mass of the particle be $\widetilde{\sigma}$ and $\widetilde{m}$, respectively. The pre- and post-collisional particle velocities of particle 1 are denoted by $\widetilde{\mathbf{c}}_1$ and $\widetilde{\mathbf{c}}_1'$, respectively. Hence, the velocity of particle 2 relative to 1 is $\widetilde{\mathbf{c}}_{21} = \widetilde{\mathbf{c}}_2 - \widetilde{\mathbf{c}}_1$. Let $\mathbf{k}_{21} = \mathbf{k}$ be the unit vector directed from the center of particle 2 to that of particle 1 at contact. The pre- and post-collisional velocities are related by the expression

$$\mathbf{k} \cdot \widetilde{\mathbf{c}}_{21}' = -e(\mathbf{k} \cdot \widetilde{\mathbf{c}}_{21}), \tag{1}$$

where e is the coefficient of normal restitution, with $0 \leq e \leq 1$; note that we restrict ourselves to perfectly smooth particles. The expression for the collisional impulse is

$$\widetilde{\mathbf{I}} = \widetilde{m}(\widetilde{\mathbf{c}}_1' - \widetilde{\mathbf{c}}_1) = \frac{\widetilde{m}}{2}(1+e)(\mathbf{k} \cdot \widetilde{\mathbf{c}}_{21})\mathbf{k}, \tag{2}$$
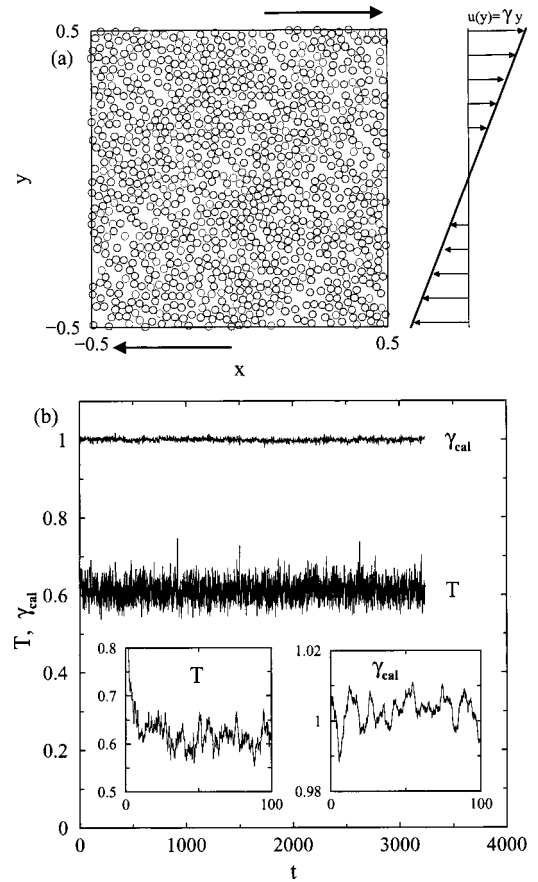
directed along $\mathbf{k}$.

FIG. 1. (a) A snapshot of the sheared granular system at steady state. The arrows indicate the displacement of the image boxes. (b) Variations of the granular energy T and the calculated shear rate γ_{cal} with time. For an explanation of the system and particle properties, see the text. The parameters for both subplots are $\nu = 0.5$, $e = 0.7$ and $N = 1024$.

A. Model system and algorithm

The system is periodic in $\widetilde{x}$-direction, i.e., a particle crossing the left/right boundary re-enters the system through the opposite boundary at the same vertical position with unchanged velocities. To impose a uniform shear rate ($\widetilde{\gamma} = \widetilde{U}/\widetilde{L}$) in the $\widetilde{y}$-direction, the top and bottom image boxes, bounding the central box, are set in motion with velocities $\widetilde{U}/2$ and $-\widetilde{U}/2$, respectively, in the streamwise direction. This is the standard approach to attain the state of uniform shear flow (USF) by imparting momemtum transfer by shearing, originally introduced by Lees and Edwards.[22] Overall, this system represents an *extended doubly-periodic* system where the periodicity in the transverse direction is in the local Lagrangian frame. In a typical simulation, the disks are initially placed randomly in the computational box, and the initial velocity field is composed of the uniform shear and a small Gaussian random part. An event-driven algorithm is then used to update the system in time, the details of which may be found in Alam and Luding.[23,24]

To ascertain whether the system has reached the statistical steady-state, the time evolution of the average fluctuation kinetic energy ("granular" energy, defined in the next section) is monitored; see Fig. 1(b). Due to the balance between the shear work and the collisional dissipation under homoge-

neous shear deformation, the granular energy attains a constant value at the steady-state. Depending on the value of the coefficient of restitution and the number of particles, it takes about a thousand collisions per particle to reach such a statistical steady-state—the lower the value of e, the more quickly the system reaches the steady-state and *vice versa*. The simulation is then allowed to run for another 15 000 collisions per particle to gather data to calculate the macroscopic quantities. A few longer runs (30 000 collisions per particle) were also checked, with no significant change on the measured quantities. Another quantity which was simultaneously monitored, along with granular energy, is the linearity of the streamwise velocity profile across the Couette gap, and we found that the calculated shear rate (i.e., the slope of the velocity profile) fluctuated around the imposed shear rate by at most 1% at densities where crystallization is not evidenced.

B. Macroscopic quantities

With $\tilde{L}$, $\tilde{\gamma}^{-1}$, $\tilde{\gamma}\tilde{L}$, and $\tilde{m}$, used as the reference length, time, velocity, and mass, respectively, the relevant dimensionless quantities are

$$\sigma = \frac{\tilde{\sigma}}{\tilde{L}}, \quad (\mathbf{c}, \mathbf{u}, \mathbf{C}) = \frac{1}{\tilde{\gamma}\tilde{L}}(\tilde{\mathbf{c}}, \tilde{\mathbf{u}}, \tilde{\mathbf{C}}), \quad \mathbf{P} = \frac{\tilde{\mathbf{P}}}{\tilde{\rho}\tilde{\sigma}^2\tilde{\gamma}^2},$$

$$T = \frac{\tilde{T}}{\tilde{\sigma}^2\tilde{\gamma}^2}, \tag{3}$$

where $\mathbf{u}$ is the "hydrodynamic" velocity, $\mathbf{C} = \mathbf{c} - \mathbf{u}$ the fluctuation (peculiar) velocity of particles, $\tilde{\rho}$ the material density of particles, $\mathbf{P}$ the stress tensor and T the granular energy.

The macroscopic stress, as measured in discrete particle simulations, is a byproduct of the particle-level mechanisms of momemtum transfer. As in the hard-core model of dense gases, the stress is the sum of its kinetic and collisional components. The former arises from the transport of momentum as the particles move through the system carrying their momentum, while the latter is due to the direct interparticle collisions. The homogeneity of the uniform shear flow allows us to calculate the stress by averaging it over the whole computational box.[3,23,24]

The stress, defined in the *compressive* sense, may be decomposed in the standard way:

$$\mathbf{P} = \mathbf{P}^k + \mathbf{P}^c = p\mathbf{1} + \mathbf{\Pi}, \tag{4}$$

where p is the pressure, $\mathbf{\Pi}$ the pressure deviator and $\mathbf{1}$ the unit tensor. From the off-diagonal components of the pressure deviator, we can calculate the *shear viscosity* which relates the rate of strain to the shear stress:

$$\mu = -\Pi_{xy} \Big/ \frac{du}{dy}. \tag{5}$$

For the steady uniform shear flow, thus, the dimensionless shear viscosity can also be interpreted as the shear stress due to our adopted scaling, $du/dy = \gamma = 1$. The diagonal compo-

nents of the pressure deviator can be nonzero, giving rise to normal stress differences. The first normal stress difference is defined as

$$\mathcal{N}_1 = \frac{(\Pi_{xx} - \Pi_{yy})}{p}. \tag{6}$$

Note that we have scaled this quantity by pressure to ascertain its relative magnitude with respect to pressure. For a standard Newtonian fluid, $\mathcal{N}_1 = 0$ and thus $\mathcal{N}_1$ is an indicator of the *non-Newtonian* character of the fluid. $\mathcal{N}_1$ can be decomposed into kinetic and collisional parts:

$$\mathcal{N}_1 = \mathcal{N}_1^k + \mathcal{N}_1^c = \frac{(\Pi_{xx}^k - \Pi_{yy}^k)}{p} + \frac{(\Pi_{xx}^c - \Pi_{yy}^c)}{p}. \tag{7}$$

Note that the *sign* of $\mathcal{N}_1$ crucially depends on the convention used to define the stress tensor. For example, in the rheology literature, stress is typically defined in the *tensile* sense.[7] A positive $\mathcal{N}_1$ for the compressive case is equivalent to its negative value for the tensile case and *vice versa*. This point should be kept in mind while making any comparison with data in the rheology literature.

From the trace of the kinetic stress tensor, $\mathbf{P}^k$, one can calculate the granular energy,

$$T = \frac{1}{2\sigma^2}\left[\frac{1}{N}\sum_{i=1}^{N}C_iC_i\right], \tag{8}$$

which is a measure of the random motion of the particles with respect to the mean motion.

There are two dimensionless control parameters: the volume fraction of particles (ν) and the coefficient of normal restitution (e). The shear rate is also a control parameter, however, due to normalization we have $\gamma = \tilde{\gamma}/\tilde{\gamma} = 1$, and changing the value of $\tilde{\gamma}$ does not influence the reported results; the imposed shear rate γ is thus kept fixed at unity. The simulations are carried out for the whole range of solid volume fractions, varying from the dilute to the dense limit, over a large range of values for the coefficient of restitution ($e = 0.3$–0.99). For most of the simulations, the number of particles are fixed to $N = 1024$, and increasing the value of N by fourfold ($N = 4096$) did not affect the reported quantities noticeably; for example, the change in $\mathcal{N}_1$ was about 4.3% and 5.1% at $\nu = 0.3$ and 0.75, respectively, for a restitution coefficient of $e = 0.9$. We note here that the system-size dependence of the rheological quantities (pressure and viscosity) is known to be strong only for a small number of particles ($N < 100$).[11,24,25]

For the typical simulation in Fig. 1(a), at steady-state, after 2×10^7 collisions, the parameter values were $\nu = 0.5$, $N = 1024$ and $e = 0.7$. The variations of the granular energy T and the calculated shear rate γ_{cal} with time are shown in Fig. 1(b), along with corresponding initial variations in two insets. (The data represent the instantaneous values of T and γ_{cal} sampled at a regular interval of 400 collisions—no time averaging is involved here.) Note that γ_{cal} was computed by binning the system into 20 equal-size bins in the transverse direction and taking averages over all particles in each bin. It is observed that the granular energy reaches its steady value ($T = 0.6121 \pm 0.022$) quickly after the initial transients and
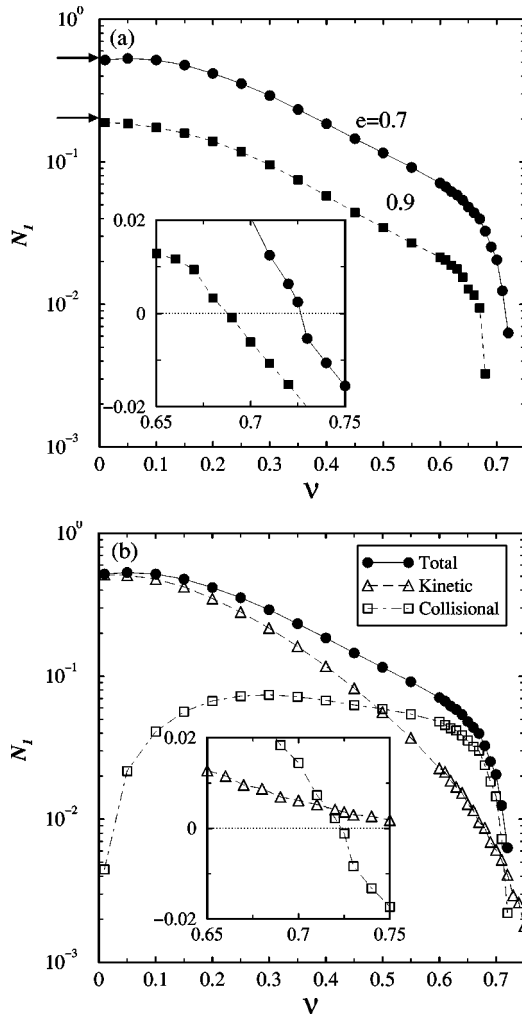
FIG. 2. (a) Variation of the first normal stress difference $\mathcal{N}_1$ with the solid volume fraction. The arrows on the left ordinate indicate corresponding analytical values for a two-dimensional granular gas. (b) Variations of $\mathcal{N}_1$, $\mathcal{N}_1^k$ and $\mathcal{N}_1^c$ with ν at $e=0.7$. In both subplots, the symbols represent the simulation data and the lines are drawn to guide the eye.

the calculated shear rate fluctuates around its imposed value ($\gamma=1$) by about $\pm 1\%$. The fluctuations in both T and γ_{cal} at steady-state are due to the finite-size of the system and diminish with increasing number of particles as $N^{-1/2}$.

III. RESULTS

For detailed results on the quantities pressure, shear viscosity and granular energy, and for their comparison with kinetic theory predictions, we refer to our recent study.[24] Here, we will mainly focus on the behavior of the first normal stress difference and its kinetic and collisional components. We also present results on the pair distribution function and the collision angle distribution to characterize microstructures. Lastly, we will present results on *crystal*-formation at high densities, signaling the coexistence of fluid and solid, complementing recent results in nonsheared systems.[26,27]

A. Normal stress difference

Figure 2(a) shows the variation of the first normal stress difference ($\mathcal{N}_1$) with density for two values of the coefficient of restitution. It is observed that $\mathcal{N}_1$ is maximum at the dilute limit and decreases thereafter with ν. The overall variation of $\mathcal{N}_1$ with density looks similar at other values of the coefficient of restitution, with a difference in the magnitude of $\mathcal{N}_1$. The inset in Fig. 2(a) shows that $\mathcal{N}_1$ decreases quite sharply in the dense limit and becomes negative at some density ($\nu = \bar{\nu}$). Increasing the value of the restitution coefficient decreases this critical density $\bar{\nu}$. The arrows on the left-ordinate indicate the asymptotic values of $\mathcal{N}_1$ for a two-dimensional granular gas in the dilute limit:[4]

$$\mathcal{N}_1 = 1.0448(1-e^2). \tag{9}$$

The anisotropy in the second moment of the fluctuation velocity is *primarily* responsible for the finite normal stress difference in the dilute limit[16,28] and this shows up only at the Burnett-order of the Chapman–Enskog expansion.[4] We should mention here that the limit $e \to 1$ is singular and the normal stress difference survives even in the elastic limit as pointed out by Goldhirsch and Sela.[4] The corresponding expression for $\mathcal{N}_1$ in a molecular gas is

$$\mathcal{N}_1 \approx 1.358 \frac{\gamma^2 \ell^2}{\langle u^2 \rangle},$$

where ℓ is the mean free path and $\langle u^2 \rangle$ is the rms of the velocity fluctuations. However, because of its extremely small magnitude under normal conditions, the normal stress difference is not *measurable* in a molecular fluid.

Previous hard-sphere simulations of Campbell and coworkers[3,19] are in *variance* with our result in that they found $\mathcal{N}_1 \to 0$ as $\nu \to \nu_{max}$. However, the soft-sphere simulations of Walton and Braun,[20] with frictional particles, support our observation that $\mathcal{N}_1$ indeed undergoes a *sign-reversal*. To better understand what is responsible for the sign-reversal of $\mathcal{N}_1$, we look at the kinetic and collisional components of the first normal stress difference. Figure 2(b) shows the variations of $\mathcal{N}_1^k$ and $\mathcal{N}_1^c$ with density at $e=0.7$. We observe that $\mathcal{N}_1^k$ is maximum at the dilute limit and decreases monotonically to zero as ν approaches the packing limit. Except for the dense limit, the overall behavior of $\mathcal{N}_1^k$ represents that of the total normal stress difference. The collisional component, $\mathcal{N}_1^c$, shows a *nonmonotonic* variation with density: $\mathcal{N}_1^c$ is zero in the dilute limit, increases with increasing ν, remains almost constant for intermediate densities, and then decays sharply in the dense limit. Interestingly, $\mathcal{N}_1^c$ becomes negative at some critical density ($\nu = \bar{\nu}$) beyond which the behavior of $\mathcal{N}_1^c$ mirrors that of $\mathcal{N}_1$ (see the inset). Thus, the normal stress behavior in the dense regime is clearly due to the anisotropy in the collisional stress.

Recall that the kinetic theory of Jenkins and Richman[16,28] predicts that $\mathcal{N}_1 \to 0$ in the dense limit. The predictions of the revised Enskog theory of Santos et al.[29] are in line with that of Jenkins and Richman, even though their kinetic model is claimed to be valid even in the crystalline-phase. Since the source of normal stress differences in all these theories is linked to the anisotropy in the
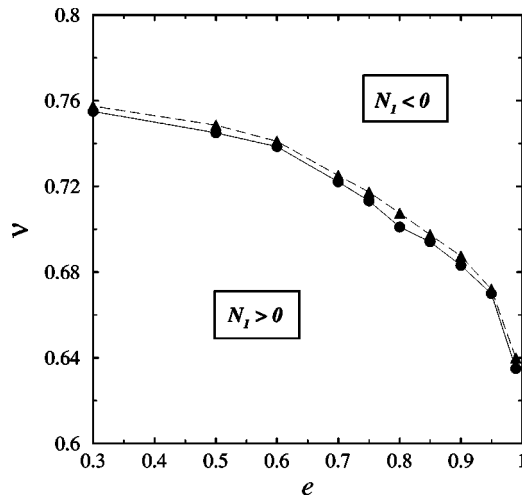
FIG. 3. The phase diagram, delineating regions of positive and negative first normal stress difference, in the (ν,e)-plane. The filled circles and triangles represent zeros of $\mathcal{N}_1^c$ and $\mathcal{N}_1$, respectively.

second moment of velocity fluctuations (which vanishes as $\nu \to \nu_{max}$), they are unable to predict the correct behavior of normal stresses in the dense limit. We would like to stress here that, as mentioned in the Introduction, many fascinating non-Newtonian effects[7] are primarily determined by the first normal stress difference and its sign. For example, the rod-climbing effect can occur in a granular fluid if $\mathcal{N}_1 < 0$, i.e., only in the dense limit (assuming that the second normal stress difference is negligible). Furthermore, having a constitutive model which reproduces the correct sign of $\mathcal{N}_1$ is also important, since it is well known in the rheology literature that the *odd* sign for $\mathcal{N}_1$ leads to the *instability* of the rest state.[30]

The sign-reversal of $\mathcal{N}_1^c$ can be succinctly presented as a phase-diagram in the (ν,e)-plane by plotting the zeros of $\mathcal{N}_1^c$ as a function of the coefficient of restitution; see Fig. 3. Below the solid line, $\mathcal{N}_1^c$ is positive, and negative above it. Also plotted in this figure is the line for the zeros of $\mathcal{N}_1$ which, as expected, lies slightly above. Thus, the first normal stress difference is zero along the solid line which may be called the *symmetry-line*. It is observed that decreasing the coefficient of restitution increases the critical density $(\bar{\nu})$ at which $\mathcal{N}_1^c$ changes sign. As we approach the elastic limit, $\bar{\nu}$ depends strongly on the value of e. We further note that as $e \to 1$, $\bar{\nu} \sim 0.62$ which is well below the freezing-point density of a two-dimensional (2-D) hard-disk fluid, $\nu_f \approx 0.70$.[26,27]

We need to mention here that the *sign-change* of $\mathcal{N}_1$ is not uncommon in other non-Newtonian fluids. For example, in non-Brownian viscous suspensions, $\mathcal{N}_1$ changes sign at a high Peclet number.[31,32] However, the reason for this effect is quite different in granular fluids as we show below.

B. Microstructural features

To understand the microstructural mechanism for the origin of the first normal stress difference and its sign-reversal, here we probe several microstructural features of a dense granular fluid.

1. Radial distribution function

Typical snapshots of the system in the dense regime are shown in Fig. 4 at four different densities with $e = 0.7$. Note that the density for the subplot, Fig. 4(c), is $\nu = 0.725$ for which $\mathcal{N}_1^c \approx 0$. Looking at the corresponding distribution of granular energies (not shown here for brevity), we could find signatures of clusters (group of particles) with lower energies surrounded by particles with higher energy. To understand the flow-microstructures and their energetics at such high densities, we need to probe the pair distribution function and similar measures for the structure of the packing.

Figures 5(a)–5(d) shows the radial distribution function $g(r)$ at four densities, with parameter values as in Fig. 4. The thin, dotted lines are data from a nonsheared, homogeneous, elastic system,[26,27] whereas the thick, solid lines represent a sheared situation with rather strong dissipation $e = 0.7$. (Note that the elastic distribution function has been measured under nonsheared periodic boundary conditions; also for e somewhat smaller than unity, the same results were obtained as long as the system remains homogeneous.) We observe that the weak difference at low density $\nu = 0.6$ grows with increasing density, concerning two aspects.

(i)   The peak value of contact in the sheared systems is always larger than that in a homogeneous system of the same density, and the difference increases strongly with density, another indicator for clustering.[33]

(ii)   The peaks and valleys, which allow us to distinguish between different lattice structures, are different in the sheared case when compared to the nonsheared situation. In the former case, peaks at $r/\sigma = 1,2,3,...$, are observed, signaling shell-formation about any test-particle. In the latter case, the peaks at $r/\sigma = 1,\sqrt{3},2,...$, indicate a crystallization transition and the development of a triangular lattice.

The peaks in the sheared situation, e.g., at $r/\sigma = 2,3$, become sharper as the density is increased, but the one at $r/\sigma = 4$ is not well-defined even at $\nu = 0.75$; higher-order peaks are almost invisible, indicating long-range disorder due to the shearing in contrast to the long-range order that evolves in the nonsheared system. The comparison between the sheared and nonsheared cases suggest that the structure-formation is much slower in a sheared fluid which, in turn, implies that, as expected, the freezing-point density of the former would be larger than that of the latter. The splitting of the second-peak in the nonsheared case corresponds to the *onset* of freezing transition;[34] with increasing density this splitting becomes much more prominent, with similar structural-features appearing at the successively higher-order peaks. For the sheared system, however, we do not observe similar splitting, rather we see a *sharp* second-peak. This also occurs for a highly inelastic sheared fluid at a much lower density;[33] hence, a sharp second peak is a signature of short-range ordering due to the dissipative particle-clustering. The higher-order peaks in the sheared case become prominent only if we go beyond $\nu = \pi/4$, which corresponds to the limit of perfect square-packing, but it is difficult to maintain homogeneous-shearing at such high den-
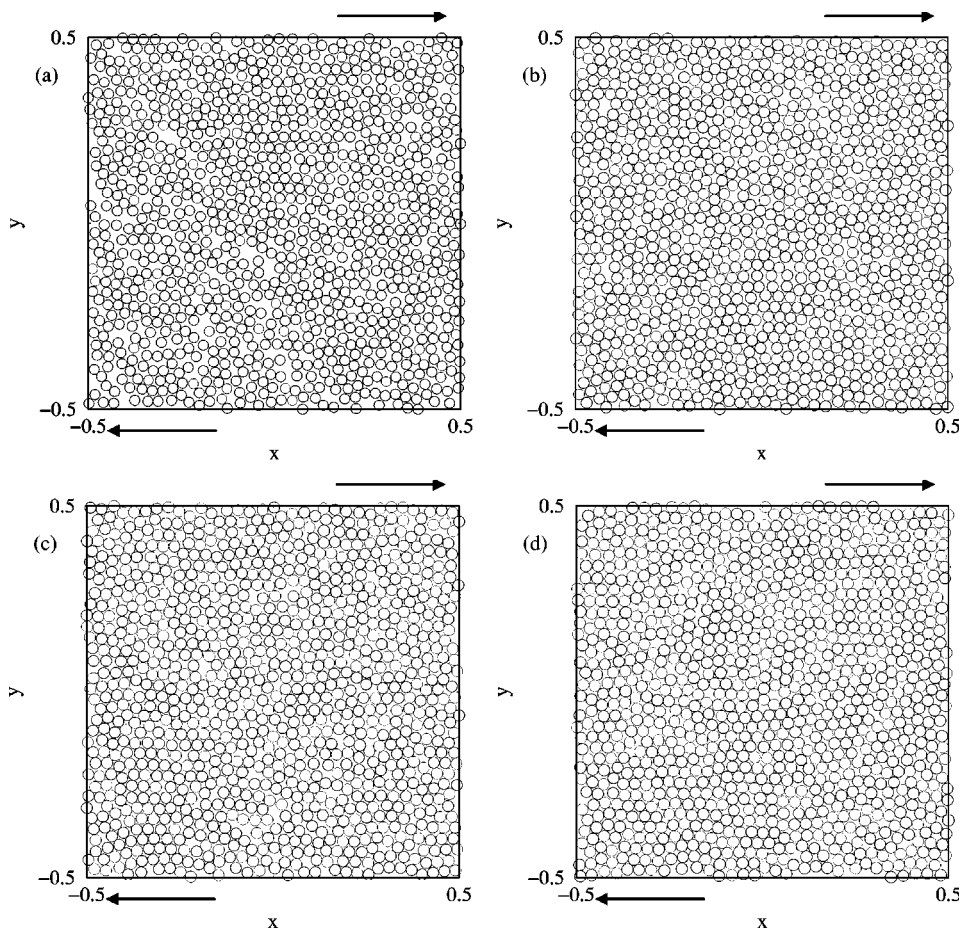
FIG. 4. Snapshots of the sheared system with $e = 0.7$ in the dense limit for different densities: (a) $\nu = 0.6$, (b) $\nu = 0.7$, (c) $\nu = 0.725$, (d) $\nu = 0.75$.

sities, because the system splits into two parts, a dense, cold, crystalline area and a dilute, hot, fluid area—see below for details.

Figure 6 shows the variations of the pressure and viscosity functions ($f_p = p/\rho T$ and $f_\mu = \mu/\rho \sigma \sqrt{T}$, respectively) with density at a restitution coefficient $e = 0.7$. We observe that both increase *monotonically* with density, much beyond $\nu = 0.7001$, and we did not find the *hysteretic* van der Waals loop in our pressure data up to $\nu = \pi/4$, another indication that the crystallization is hindered/delayed by shear. These observations, together with our result that in the elastic limit $\mathcal{N}_1$ changes sign at a much lower density ($\nu \approx 0.62$; see Fig. 3) than the corresponding freezing-density, suggest that the sign-reversal of $\mathcal{N}_1$ is not related to the freezing-transition.

2. Collision angle distribution

Associated with the *sign-reversal* of the first normal stress difference is a change in the relative magnitudes of the normal stress components (P_{xx} and P_{yy}). Subtle changes in the direction and magnitudes of the collisional-mode of momemtum transfer could influence the individual components of the stress tensor. In order to test this hypothesis, we focus on the collision angle distribution function, $C(\theta)$, which is defined such that $C(\theta)d\theta$ is the probability of collisions occurring at an angle lying between θ and $\theta + d\theta$, with the angle θ being measured in the anticlockwise direction from the positive x-axis (see Fig. 13 later). For a fluid in equilibrium, all collisions are equally likely, and hence $C(\theta)$ is a

uniform function of θ, i.e., $C(\theta) = 1/\pi \approx 0.318309$. For a nonequilibrium system (e.g., shear flow), however, preferred collisions are dictated by the nature of the external field, leading to an anisotropic distribution for $C(\theta)$.[35–38] Following Savage and Jeffrey[36] and Campbell and Brennen,[37] an explicit expression for $C(\theta; \nu, e)$ can be derived for the case of uniform shear flow as detailed in the Appendix. Note that the angular dependence of $C(\theta; \nu, e)$ will be modified by both the density and the restitution coefficient.

Figure 7 shows the comparison of our simulation data on $C(\theta)$ with the theoretical predictions of Eq. (A9) for two different values of the restitution coefficient at a density $\nu = 0.6$. It is observed that the probability of collisions is higher on the *upstream*-faces of the colliding particles, i.e., for $\theta \in [\pi/2, \pi]$ and $\theta \in [-\pi/2, 0]$ (i.e., the hatched-areas on the test-particle in Fig. 13). This is a consequence of the imposed shear-field which compresses the flow-structure along the $3\pi/4$-direction and stretches it along the $\pi/4$-direction. Regarding the comparison with theory, there is, clearly, a phase-difference between theory and simulation, and the overall agreement is only qualitative.

Note in Fig. 7 that the probability of collisions on the upstream-faces increases further as the restitution coefficient increases. This, in turn, suggests that particle motion becomes more *streamlined* (i.e., along the streamwise direction) with increasing dissipation levels, which will naturally lead to a reduction in the transverse component of the fluctuation velocities of the particles. Thus, the *macroscopic*
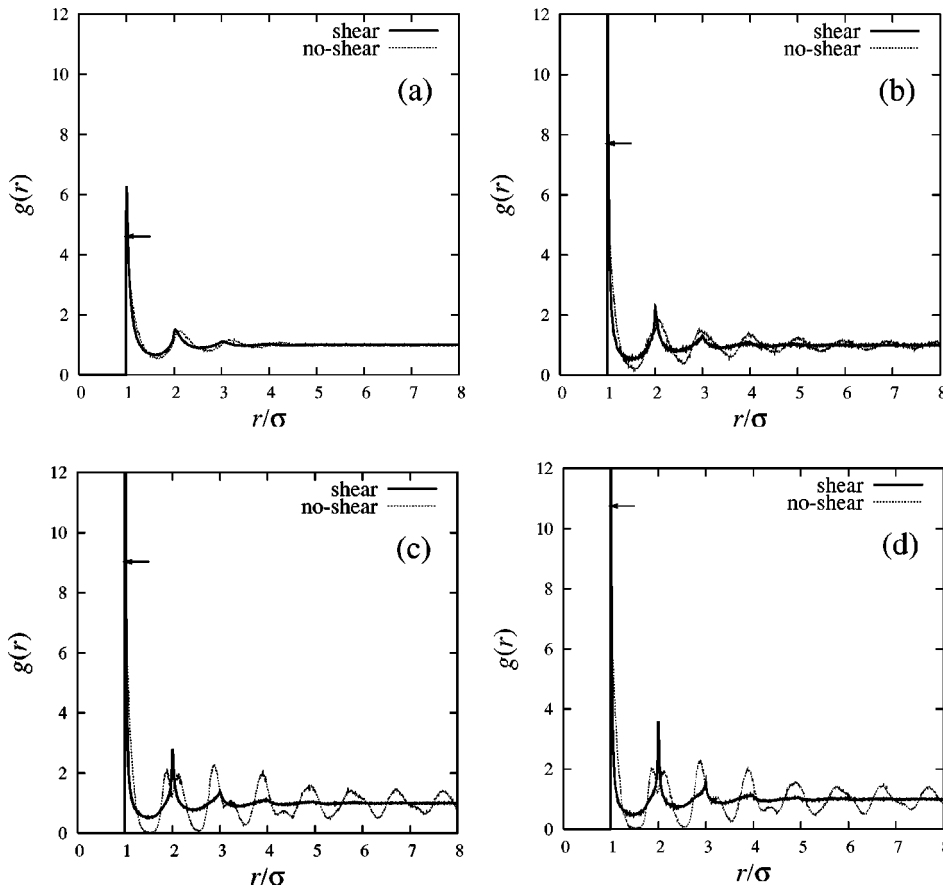
FIG. 5. Radial distribution function $g(r)$ plotted against the normalized distance r/σ from sheared simulations with dissipation $e = 0.7$ (solid lines) and from homogeneous, nonsheared situations with $\gamma = 0$ and $e = 1$ (dotted lines): (a) $\nu = 0.6$, (b) $\nu = 0.7$, (c) $\nu = 0.725$, (d) $\nu = 0.75$. The arrows indicate the peak values of $g(r)$ at contact for the homogeneous system.

manifestation of such *microscopic* streamlined-motion would be an increase in the magnitude of the kinetic component of the first normal stress difference ($\mathcal{N}_1^k$).

Turning our attention to the range of densities where $\mathcal{N}_1$ undergoes a sign-reversal, we show the collision angle distributions $C(\theta)$ in Fig. 8 as polar plots with $e = 0.7$; the corresponding densities are as in the subplots of Fig. 4. It is observed that the *anisotropic* structure of $C(\theta)$ gets further modified in this regime, with distinct peaks appearing near

$\theta = 0$ and $2\pi/3$ [see Fig. 8(b)]. While the peak at $\theta = 0$ corresponds to *head-on* collisions between particles in the same-layer, the one at $\theta = 2\pi/3$ clearly signals the *onset* of triangular-structure formation. Another noteworthy point is that the collisions on the downstream-faces of the colliding particles are *rare* at these densities and hence $C(\theta)$ can be approximated solely by its contributions from the second-
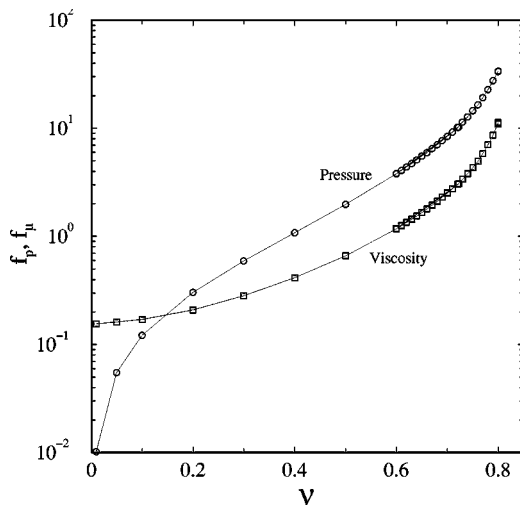

FIG. 6. Variations of the pressure and viscosity functions with density at $e = 0.7$: $f_p = p/\rho T$ and $f_\mu = \mu/\rho\sigma\sqrt{T}$. The lines are drawn to guide the eye.
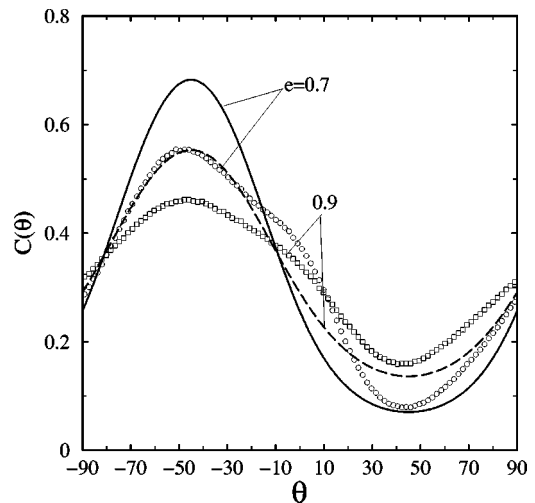

FIG. 7. Distribution of collision angles $C(\theta)$ for different coefficient of restitutions at $\nu = 0.6$. The symbols represent simulation data and the lines theoretical predictions.
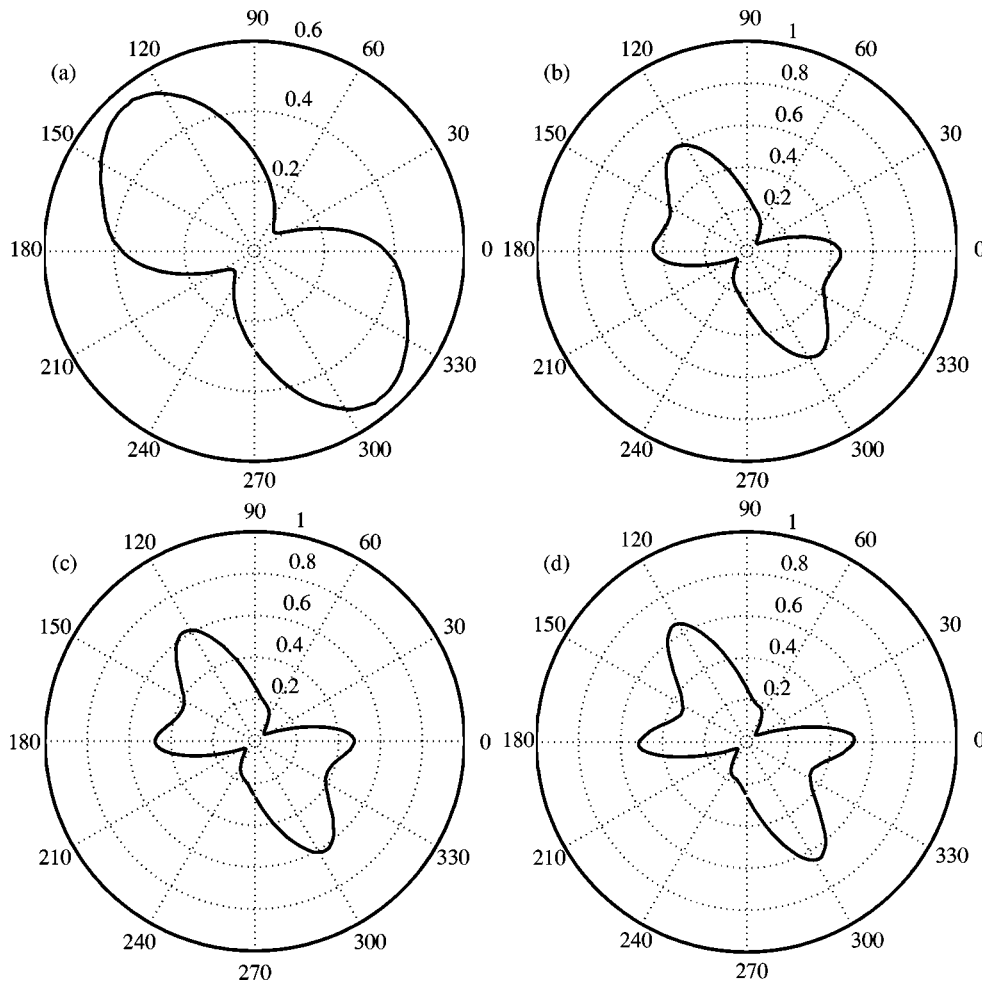
FIG. 8. Polar plots of the collision angle distribution for different densities at $e=0.7$: (a) $\nu=0.6$, (b) $\nu=0.7$, (c) $\nu=0.725$, (d) $\nu=0.75$.

and fourth-quadrants ($\theta \in [\pi/2, \pi]$ and $\theta \in [-\pi/2, 0]$, respectively).

Since the momentum transfer occurs mainly due to collisions in the dense regime, the stress tensor can be approximated by

$$\mathbf{P} \sim \int (\mathbf{k} \otimes \mathbf{k}) C(\theta) d\theta,$$

where $\mathbf{k}$ is the unit vector joining the line of centers of the two colliding disks. Assuming now that all the collisions would occur at some average collision angle θ_{av} so that $C(\theta) = C(\theta_{av})$, and recalling that $C(\theta)$ is well represented in this regime by restricting θ only in the second- and fourth-quadrants, the expression for the first normal stress difference simplifies significantly to

$$\mathcal{N}_1 \sim [(\mathbf{k} \otimes \mathbf{k})_x - (\mathbf{k} \otimes \mathbf{k})_y]_{\theta = \theta_{av}} C(\theta_{av}). \qquad (10)$$

It is trivial to check that $\mathcal{N}_1 = 0$ at $\theta_{av} = -\pi/4$. From our simulation data, we have calculated θ_{av} by averaging $C(\theta)$ over the second- and fourth-quadrants, whose variation with density is plotted in Fig. 9 for two restitution coefficients. It is observed that θ_{av} crosses through $-\pi/4$ (i.e., $3\pi/4$) at around the critical density $\bar{\nu}$ for all restitution coefficients. For example, $\theta_{av} \approx -45.16°$ and $-45.04°$ at $\bar{\nu} = 0.725$ and

0.67, respectively, where $\mathcal{N}_1$ changes sign. Thus, the microstructural signature of the sign-reversal of $\mathcal{N}_1$ is directly correlated with the *average* collision angle being greater or less than $-\pi/4$ (or $3\pi/4$).
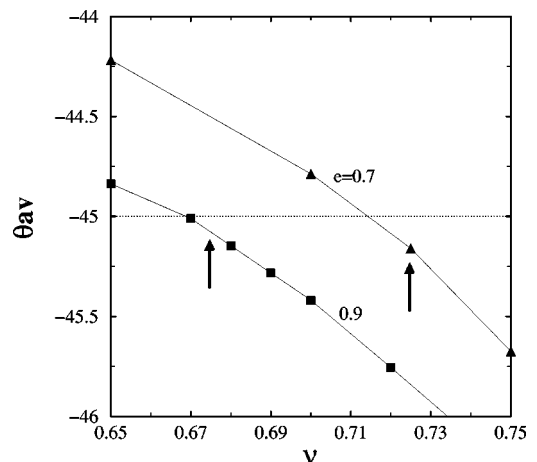

FIG. 9. Variations of the average collision angle θ_{av} with density for different restitution coefficients. The arrows indicate densities where $\mathcal{N}_1 \approx 0$. The lines joining the data points are to guide the eye.
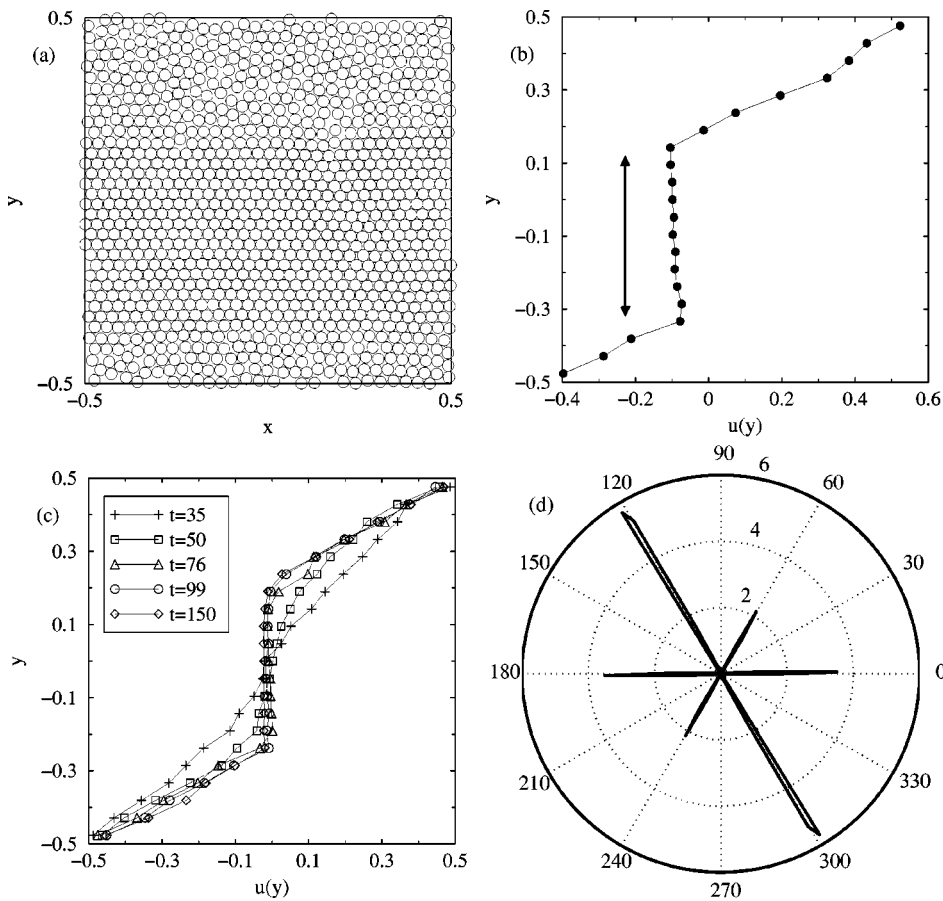
FIG. 10. Evidence of *crystallization* in a sheared dense granular fluid at $\nu = 0.8$ and $e = 0.9$. (a) Particle distribution and (b) streamwise velocity at $t = 390$; (c) evolution of streamwise velocity at early times; (d) collision angle distribution.

C. Crystallization: Fluid–solid coexistence

Figure 10(a) shows a snapshot of the system at the steady state with parameter values being set to $\nu = 0.8$ and $e = 0.9$. It is observed that a solid-layer coexists with two fluidized zones on either side of it. A closer look into the solid-layer reveals that the particles are arranged in a triangular-packing, representing a *crystal*, and thus we have a clear evidence for *fluid–solid* coexistence. The corresponding *instantaneous* streamwise velocity profile at $t = 390$ (i.e., the image-boxes have moved 390 strain units from their original position) is shown in Fig. 10(b); the coarse-graining is done by binning the system into 20 equal-size bins in the transverse direction and then taking averages over all the particles in each bin. Clearly, the shearing is *inhomogeneous* across the Couette-gap: the crystal is aligned along the streamwise direction and hence we call it a *layered*-crystal; the shear-rate in the fluidized regimes on either side of the crystal is almost uniform. Note that the *asymmetric* nature of the velocity profile also signals the breakdown of the Lees–Edwards boundary condition as a motor for the homogeneous shear. The formation and the time-evolution of this crystal can be ascertained from Fig. 10(c) which shows the corresponding evolution of the streamwise velocity at early times. We observe that the crystal has fully formed at $t = 76$, and the velocity profile remains antisymmetric about $y = 0$ until $t = 150$. With further time-evolution, however, the crystal does not remain stationary in the transverse direction, rather it moves slowly with particles diffusing across the fluid–solid interface. The overall life-time of this crystal is several orders of magnitude larger than the external time-scale γ^{-1}, imposed by the shear. The corresponding collision-angle distribution $C(\theta)$ in Fig. 10(d) shows three distinct peaks at $\theta = 0$, $\pi/3$ and $2\pi/3$. Note that the peak at $\theta = \pi/3$ does not exist in the fluid phase [refer to Fig. 8(a)], and this provides evidence that the particles in the crystalline-phase are arranged in the triangular-packing structure. The large area of the crystalline phase as well as its relatively large value of solids fraction (hence, small mean free time) further suggest that most of the collisions occurred in the crystalline-phase.

We should remark here that, at such high densities, the *inelastic collapse*[39–41] would eventually terminate the evolution of the system. We used the TC-model[40] to avoid inelastic collapse, but could not altogether eliminate it within the crystal after some time. But the important point to note is that the crystalline-phase can be maintained for a long period of time ($t > 100$ strain units), and hence the reported results are not transient effects.

Analogous plots for a nearly elastic system ($e = 0.99$) are shown in Figs. 11(a)–11(c) for the same density $\nu = 0.8$. The overall features are similar to that for $e = 0.9$, but the width of the crystalline zone is a little larger. By decreasing the dissipation-level to $e = 0.7$, we did not observe crystal formation, with other parameters being fixed; by increasing the system-size to $N = 4096$, however, we observed layered crystal at $e = 0.7$. Thus, the formation of such
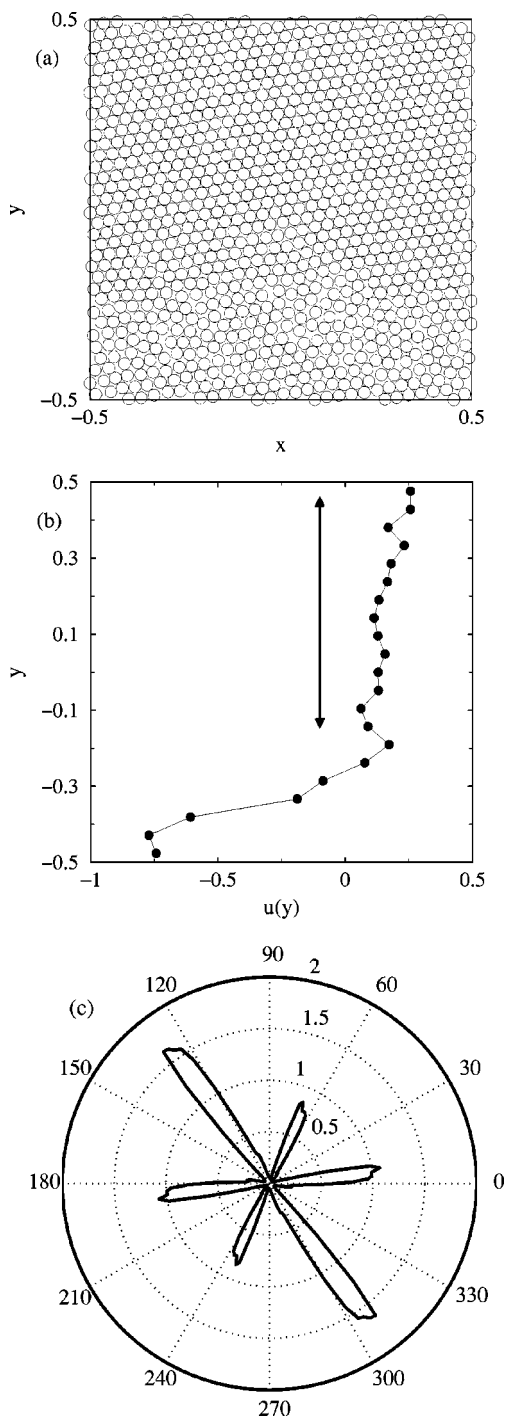
Phys. Fluids, Vol. 15, No. 8, August 2003

First normal stress difference and crystallization 2307

FIG. 11. Effect of the coefficient of restitution on *crystallization*: $\nu = 0.8$ and $e = 0.99$. (a) Particle distribution and (b) streamwise velocity at $t = 150$; (c) collision angle distribution.

layered-crystalline structure depends crucially on the system size and the dissipation level: *the larger the system-size and/or the weaker the dissipation, the more susceptible the system is to crystallize.*

Note that even if we are well below the limit of perfect square-packing ($\nu_{sp} = \pi/6 \approx 0.785$), the system could crystallize if the dissipation-levels are low; for example, we observed layered crystalline structures at $\nu = 0.75$ with $e = 0.99$ and $N = 4096$. Decreasing the coefficient of restitution to $e = 0.9$, the flow-field remained homogeneous. Thus,

our layered crystalline structures appear to be tied to a *long-wave* instability of the elastic hard-sphere fluids.[56] Since our results are not driven by the inelastic dissipation, they are distinctly different from the layered shear-banding patterns, as predicted by the kinetic theory models,[15,42,43] in granular Couette flows. Having said that we need to mention that such *dissipative* layering patterns (i.e., those which become stronger with increasing dissipation levels[15]) were also found in simulations of a dilute sheared granular fluid,[43] but the simulations were allowed to evolve from an *unsheared* initial configuration with a special kind of boundary condition. In contrast, all our simulations started from a uniform shear condition. In the present contribution, we have mainly focused on the nondissipative layering in the dense limit, and the related issues of dissipative layering are relegated to a future study.

Before moving further, we make a qualitative comparison with the earlier simulation work of Campbell and Brennen[37] on the bounded Couette flow of inelastic, frictional hard disks. They also reported a similar layered-microstructure but due to the small system-size ($N = 40$) and boundary-effects (they considered a shear-flow bounded by frictional walls), the distinct shear-band formation that we have reported is not evident in the snapshots of their simulations. Nevertheless, we believe that our results are akin to that reported by Campbell and Brennen. One of the referees has drawn our attention to the recent work of Campbell[44] who probed the dense limit of a three-dimensional Couette shear flow using soft-sphere simulations. He was able to maintain uniform shearing even at a density of $\nu = 0.62$, but beyond that he reported shear-band formation in that the flow-field degenerates into sheared and nonsheared zones in the gradient direction. This simply suggests that one can maintain uniform shearing in a three-dimensional geometry even beyond the analogous square-packing limit ($\phi = \pi/4 \approx 0.52$) since the particles have now an additional degree of freedom, orthogonal to the shear plane, to rearrange themselves. Moreover, most of Campbell's simulations were done with 1000 particles [equivalently, 100 particles in two dimensions (2D)] at a restitution coefficient of 0.7. With these parameter values, we did not find layered crystals at $\nu = 0.8$ in two dimensions (see the discussion in the next section).

Shear-induced ordering and Reynold's dilatancy

One of the referees has drawn our attention to the recent work of Lutsko[45] who studied the shear-induced ordering in a low-density ($\nu \approx 0.26$) elastic hard-sphere fluid. The earliest simulations of Erpenbeck[46] on 3-D elastic hard-sphere fluids showed that at high shear rates the system breaks down into ordered (solid) and disordered (fluid) phases in the direction of the mean vorticity (i.e., normal to the shear-plane). This induces a long-range two-dimensional ordering, called a *string-phase*, in the shear-plane. More importantly, such ordering occurs only for a range of shear-rates—the lower the density, the larger this shear-rate interval. However, the latter work of Evans and Morriss[47] showed that the disorder–order transition of Erpenbeck arises due to the profile-biased-thermostat[47] since the string-phase vanishes completely when a profile-unbiased-thermostat[47] is used.
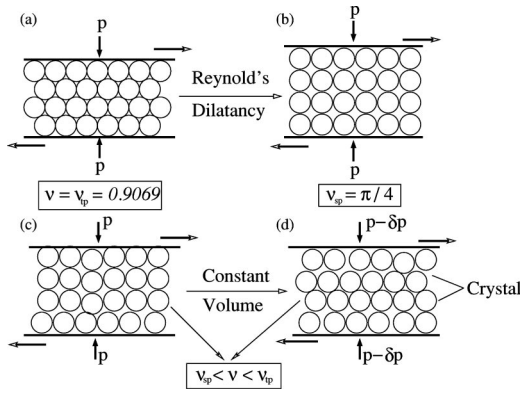
FIG. 12. A schematic diagram to explain Reynold's dilatancy in the Couette shear flow.

Thus, the shear-induced-ordering in elastic hard-sphere fluids appears to depend on the choice of the thermostat. Note further that all the above works probed moderately dense systems only, well below the corresponding square-packing limit. Now to compare these results with our observations in granular fluids, we first need to define an equivalent shear rate since the granular energy and the shear rate are dependent on each other for the latter system. From the energy balance equation, it is trivial to show that the granular energy has the following functional relation with the shear rate and the restitution coefficient:

$$T \propto \frac{\gamma^2}{1 - e^2} \propto \gamma^{*2},$$

where $\gamma^* = \gamma/(1 - e^2)^{1/2}$ is defined as the *reduced shear rate*. In the quasielastic limit ($e \to 1$) the reduced shear rate (and hence the granular energy) approaches infinity, which is equivalent to the high shear-rate limit of an elastic hard-sphere fluid. Since we observed layered crystalline structures only in the quasielastic limit, we may thus conclude that such structures would also persist in elastic hard-disk fluids at large shear rates.

It is interesting to ask whether the layered crystalline-structures of Figs. 10 and 11 are, in any way, related to the concept of the Reynold's dilatancys[17,18] which is explained schematically in Fig. 12. The top two sketches depict the classical *constant-load*[48] shear-cell experiment (in two-dimensions) in which the material is subjected to a constant normal load. Figure 12(a) corresponds to an ideal situation of maximum packing, with the particles being arranged in a triangular lattice ($\nu = \nu_{tp} = \pi/2\sqrt{3}$). Clearly, in this situation the top and the bottom plates of the shear cell will simply slide over the material, without deforming it. However, if one of the plates is allowed to move in the vertical direction and thereby allowing the particles to rearrange themselves, e.g., as in Fig. 12(b), the material can be deformed even homogeneously (if $\nu \leq \nu_{sp} = \pi/6$). This is the *shear-coupled volume change*, commonly known as the Reynold's dilatancy. Note, however, that our simulations mimic *constant-volume* experiments, since the volume of the computational box remains fixed [see Figs. 12(c) and 12(d)]; but, of course, now the pressure (i.e., normal load) can vary in response to

particle motions inside the shear cell. For this case also, the uniform shearing is possible if and only if the overall density remains below the square-packing limit ($\nu < \nu_{sp}$). However, for densities above this value ($\nu_{sp} < \nu < \nu_{tp}$), the shearing can be started only if we allow the particles to rearrange themselves. This is possible if a part of the system becomes denser, allowing *free* volumes to the rest of the system which is nothing but Reynold's dilatancy too. Hence, we will end up with a crystalline-phase coexisting with a fluid phase, a typical example of which is shown schematically in Fig. 12(d). Thus, the phenomenon of Reynold's dilatancy, for densities $\nu_{sp} < \nu < \nu_{tp}$, would make the *ordering* transition, as depicted in Figs. 10 and 11, more prominent, and this effect would be much stronger in two dimensions.

IV. CONSEQUENCES FOR THE CONSTITUTIVE MODELING: RELAXATION MODELS

Here we attempt to describe the normal-stress behavior of a granular fluid using the standard relaxation-type models. Prior literature on the dense-gas kinetic theory, which forms the foundation of theoretical developments of granular fluids in the *rapid-shear* regime, indicates that such a stress relaxation mechanism does also exist in granular fluids.[49–51] The relaxation-type models are routinely used to describe the non-Newtonian behavior of viscoelastic/viscoplastic materials, and hence might be apt for granular fluids in the dense limit as well. The recent work of Zhang and Rauenzahn[52,53] clearly shows that such viscoelastic stress relaxation mechanism exists in dense granular flows. Following a rigorous statistical mechanical procedure, they derived an evolution equation for the collisional stress tensor which boils down to a frame-indifferent viscoelastic model, with the Jaumann derivative appearing directly without appealing to objectivity arguments.

Let us consider the viscoelastic relaxation approximation suggested recently by Jin and Slemrod[51] to regularize the Burnett-order equations of Sela and Goldhirsch[5] for a low-density granular fluid. Their proposed equation for the pressure deviator, in our notation, is

$$\mathbf{\Pi} + \tau_1 \left(\frac{D\mathbf{\Pi}}{Dt} - \mathbf{L}^T \cdot \mathbf{\Pi} - \mathbf{\Pi} \cdot \mathbf{L} + \frac{2}{d} \mathrm{tr}(\mathbf{\Pi} \cdot \mathbf{L}) \mathbf{1} \right)$$
$$+ \tau_2 \left(\mathbf{S} \cdot \mathbf{\Pi} + \mathbf{\Pi} \cdot \mathbf{S} - \frac{2}{d} \mathrm{tr}(\mathbf{\Pi} \cdot \mathbf{S}) \mathbf{1} \right) = \mathbf{\Pi}^{eq}, \quad (11)$$

where

$$\mathbf{\Pi}^{eq} = -2\mu \mathbf{S} - (\lambda \nabla \cdot \mathbf{u}) \mathbf{1} + \mathbf{\Pi}_2 + \mathbf{\Pi}_3,$$

$$\mathbf{S} = \frac{1}{2} (\mathbf{L} + \mathbf{L}^T) - \frac{1}{d} (\nabla \cdot \mathbf{u}) \mathbf{1},$$

$$\mathbf{L} = (\nabla \mathbf{u})^T = \left(\frac{\partial u_i}{\partial x_j} \right),$$

$$\lambda = \left(\zeta - \frac{2}{d} \mu \right),$$

$$\tau_1 = 0.3211 \left(\frac{\mu}{p} \right),$$

$$\tau_2 = 0.58775\left(\frac{\mu}{p}\right).$$

Here τ_1 and τ_2 are relaxation times, d the dimensionality of the system, $\mathbf{L}$ is the velocity gradient, $\mathbf{S}$ the deviatoric part of the rate of strain tensor, μ the shear viscosity, ζ the bulk viscosity and $\mathbf{1}$ the identity tensor; $\mathbf{\Pi}_2$ and $\mathbf{\Pi}_3$ are higher-order terms, explicitly written down in Jin and Slemrod.[51] Note that both relaxation times are proportional to the ratio of the shear viscosity and the pressure, and hence proportional to the mean free time. In the limits of τ_1, $\tau_2 \to 0$ and $\mathbf{\Pi}_2$, $\mathbf{\Pi}_3 \to 0$, we recover the standard Newtonian model for the stress tensor.

Neglecting the higher-order terms, an expression for the first normal stress difference can be obtained for the steady uniform shear flow:

$$\mathcal{N}_1 = \left[\frac{4\tau_1}{2(1+\tau_1^2)+\tau_2(1+\tau_1-\tau_2)}\right]\left(\frac{\mu}{p}\right) > 0. \tag{12}$$

This quantity is always positive, as in our simulation results for dilute flows, if the two relaxation times are of the same order.

It is important to note that the above evolution equation does not satisfy the *principle of material frame indifference* (MFI) which states that the constitutive laws should be *invariant* under rigid-rotation.[7,8] The scalar field ϕ, the vector field $\mathbf{v}$ and the tensor field $\mathbf{\Pi}$ are called *frame-indifferent* or *objective* if the following relations hold for all t:

$$\phi'(\mathbf{x}',t') = \phi(\mathbf{x},t), \tag{13}$$

$$\mathbf{v}'(\mathbf{x}',t') = \mathbf{Q}(t)\mathbf{v}(\mathbf{x},t), \tag{14}$$

$$\mathbf{\Pi}'(\mathbf{x}',t') = \mathbf{Q}(t)\mathbf{\Pi}(\mathbf{x},t)\mathbf{Q}(t)^T, \tag{15}$$

where ϕ, $\mathbf{v}$ and $\mathbf{\Pi}$ and ϕ', $\mathbf{v}'$ and $\mathbf{\Pi}'$ are defined in two different frames, $\mathcal{F}$ and $\mathcal{F}'$, respectively, and $\mathbf{Q}(t)$ is a proper orthogonal tensor. Here $\mathcal{F}' \in \mathcal{E}(\mathcal{F})$, with $\mathcal{E}(\mathcal{F})$ denoting the set of all frames obtainable from a given frame $\mathcal{F}$ by observer transformations. That the stress-tensor in a granular gas is not a frame-independent quantity (as in the hard-sphere gas[54,55]) is well-known. Since the kinetic component of the first normal stress difference remains positive at all densities, the kinetic stress tensor can be modeled using a nonobjective equation as discussed above. For the collisional stress tensor, one can postulate a similar evolution equation as in Eq. (11), but τ_1 must be multiplied by a factor which must change sign at the critical density. However, this equation would remain frame-dependent even in the dense limit. Thus, if one has to recover the Boltzmann-limit of relaxation-type equations, a frame-indifferent approach does not appear to work.

A question now arises as to the possibility of modeling normal stress differences using the standard frame-indifferent relaxation-type models. The simplest way is to use either the *lower-convected* or the *upper-convected* equations for the pressure deviator:

$$\mathbf{\Pi} + \alpha(\nu,e)\tau\left(\frac{D\mathbf{\Pi}}{Dt} + \left\{\mathbf{L}^T\cdot\mathbf{\Pi} + \mathbf{\Pi}\cdot\mathbf{L} - \frac{2}{d}\mathrm{tr}(\mathbf{\Pi}\cdot\mathbf{L})\mathbf{1}\right\}\right)$$
$$= -2\mu\mathbf{S} - (\lambda\boldsymbol{\nabla}\cdot\mathbf{u})\mathbf{1}, \tag{16}$$

$$\mathbf{\Pi} + \alpha(\nu,e)\tau\left(\frac{D\mathbf{\Pi}}{Dt} - \left\{\mathbf{L}\cdot\mathbf{\Pi} + \mathbf{\Pi}\cdot\mathbf{L}^T - \frac{2}{d}\mathrm{tr}(\mathbf{\Pi}\cdot\mathbf{L})\mathbf{1}\right\}\right)$$
$$= -2\mu\mathbf{S} - (\lambda\boldsymbol{\nabla}\cdot\mathbf{u})\mathbf{1}, \tag{17}$$

respectively. Here $\alpha(\nu,e)$ is an empirical constant, dependent on both the density and restitution coefficient. For both cases, the first normal stress difference is

$$\mathcal{N}_1 = -\frac{2\tau\alpha}{1+\tau^2\alpha^2}\left(\frac{\mu}{p}\right). \tag{18}$$

Clearly, if $\alpha(\nu,e)$ is obtained from simulation, its sign-reversal would also correspond to the sign-reversal of $\mathcal{N}_1$. Comparing the Jin–Slemrod equation with its corresponding frame-indifferent analog (lower-convected model), we conclude that the loss of frame-indifference shows up as a *sign-change* of the first normal stress difference. It would be interesting to investigate whether one could relax the Sela–Goldhirsch equations[4] using a frame-indifferent approach without violating the entropy inequality.[51]

Similarly, one could postulate evolution equations using other objective derivatives. In this regard, the co-rotational Jeffrey's model seems to be the ideal choice:

$$\mathbf{\Pi} + \tau_1(\nu,e)\frac{\mathcal{D}\mathbf{\Pi}}{\mathcal{D}t} = -2\mu\left(\mathbf{S} + \frac{\lambda}{2\mu}(\boldsymbol{\nabla}\cdot\mathbf{u})\mathbf{1} + \tau_2(\nu,e)\frac{\mathcal{D}\mathbf{S}}{\mathcal{D}t}\right), \tag{19}$$

with $\mathcal{D}/\mathcal{D}t$ being the Jaumann derivative.[7] The corresponding first normal stress difference is

$$\mathcal{N}_1 = -\frac{2(\tau_1 - \tau_2)}{1+\tau_1^2}\left(\frac{\mu}{p}\right), \tag{20}$$

which is positive/negative depending on whether τ_1 is less/greater than τ_2. Thus, the frame-indifferent relaxation models are able to predict positive and negative first normal stress differences. (For the steady homogeneous shear flow, one can also model positive/negative normal stress differences by postulating a general orthonormal basis, generated by the nilpotent basis tensors, which satisfies the objectivity requirement; for related issues, the reader is referred to Goddard.[8])

V. SUMMARY AND CONCLUSION

We have probed the non-Newtonian behavior and the incipient crystalline-phase in a sheared, monodisperse, two-dimensional granular fluid. The standard event-driven technique is used to simulate a box of hard-disks under homogeneous shear deformation. The information about the stress tensor is obtained by decomposing it in the standard way: $\mathbf{P} = p\mathbf{1} + \mathbf{\Pi}$, where p is the pressure and $\mathbf{\Pi}$ the pressure deviator. The non-Newtonian behavior is quantified in terms of the first normal stress difference: $\mathcal{N}_1 = (\Pi_{xx} - \Pi_{yy})/p$.

The granular fluid is non-Newtonian with a measurable first normal stress difference ($\mathcal{N}_1$) which is *positive* (if the stress is defined in the *compressive* sense) in the dilute limit. Interestingly, however, $\mathcal{N}_1$ *changes* from positive to negative at a critical density in the dense regime. By decomposing $\mathcal{N}_1$ into the kinetic and collisional contributions, $\mathcal{N}_1 = \mathcal{N}_1^k + \mathcal{N}_1^c$, we found that while $\mathcal{N}_1^k$ is always positive and decays to zero in the dense limit, $\mathcal{N}_1^c$ has a *nonmonotonic* variation with density. In particular, $\mathcal{N}_1^c$ increases from zero in the dilute limit as ν increases, reaches a maximum at some value of ν and then decreases, eventually becoming *negative* in the dense limit. The density at which $\mathcal{N}_1^c = 0$ ($\nu \equiv \bar{\nu}$) depends crucially on the level of micro-scale dissipation; in particular, $\bar{\nu}$ increases as the coefficient of restitution decreases. We have constructed a phase-diagram in the (ν, e)-plane by identifying the regions where $\mathcal{N}_1$ is positive/negative.

We have shown that the *origin* of the first normal stress difference, in the dense limit, is tied to shear-induced collisional anisotropies. The underlying mechanism is distinctly different from that is known for a dilute granular gas[4,16] where the anisotropy in the second moment of the fluctuation velocity, which is a Burnett-order effect, gives rise to normal stress differences.

At the micro-level, the particles undergo reorganization as the dense-limit is approached. The signatures of microstructural-reorganization have been captured by probing the collision-angle distribution, $C(\theta)$, which is *anisotropic* due to the presence of the mean shear. In particular, we have found that the topology of the anisotropic-structure of $C(\theta)$ changes, with collisions occurring at certain preferred angles on the upstream-faces of the colliding pairs. The *sign-reversal* of $\mathcal{N}_1$ is correlated with a preferred value of the average collision angle, $\theta_{\mathrm{av}} = \pi/4 \pm \pi/2$, averaged over the *upstream*-faces of the colliding particles.

The time evolution of the sheared granular fluid leads to *crystallization* in the dense limit, signaling the *coexistence* of fluid and solid. The particles are arranged in a triangular-packing inside the crystal, and it moves as a *layer* in the streamwise direction. The formation of such layered-crystalline structure depends crucially on the system size and the dissipation level: the larger the system-size and the weaker the dissipation, the more susceptible the system is to crystallize. This appears to be related to a long-wave instability[56] of the elastic hard-sphere fluids.

The present work clearly shows that the available kinetic-theory-based rheological models for granular fluids are not adequate to predict the behavior of the first normal stress difference in the dense limit. Certain microstructural-features, like the preferred distribution of collisions which eventually leads to crystal-formation, should be incorporated into the theory. At such high densities, many-body effects (both positional and velocity correlations) are important[41,57] and the appropriate kinetic description is the BBGKY-hierarchy.[57] To incorporate the observed normal stress behavior into the framework of plausible constitutive models, we showed that the standard frame-indifferent relaxation-type models can be used to model both positive and negative first normal stress differences. In this regard,
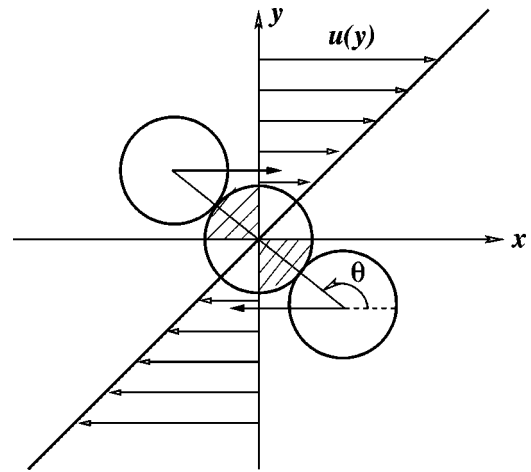

FIG. 13. A schematic of the possible collision angles θ in uniform shear flow; θ is measured anticlockwise from the positive x-axis. Note that the collisions are more likely to occur in the second ($\pi/2 < \theta < \pi$) and fourth ($3\pi/2 < \theta < 2\pi$) quadrants of the colliding disks, represented by the hatched areas of the test-particle.

the two-parameter Jeffrey's model[7] appears to be the ideal choice; however, we are unable to recover the corresponding Boltzmann limit which is known to be nonobjective. On the whole, we believe that a lot remains to be done for a better understanding of the dense-phase rheology of granular fluids even in the hard-sphere limit.

ACKNOWLEDGMENTS

APPENDIX: SHEAR-INDUCED ANISOTROPY AND THE COLLISION ANGLE DISTRIBUTION

Here we are interested in the shear-induced anisotropy of the collision angle distribution of an inelastic hard-disk fluid. Following Savage and Jeffrey,[36] an expression for the collision angle distribution $C(\theta)$ is derived, which is compared with the simulation data in Sec. II B 2.

To calculate the probablility of collisions at a specific angle θ, we focus on Fig. 13 with two particles colliding at $\mathbf{r}$. Note that θ is measured anticlockwise from the positive x-axis. For collisions to occur in a time δt, the center of particle 1 must lie inside the volume $\sigma \delta \mathbf{k} (\mathbf{q} \cdot \mathbf{k}) \delta t$, where $\mathbf{q} = \mathbf{c}_1 - \mathbf{c}_2$ is the relative velocity of the colliding pair. Thus the expected total number of collisions (per unit time and unit area) with the line of centers $\mathbf{k}$ lying between $\mathbf{k} - \delta \mathbf{k}/2$ and $\mathbf{k} + \delta \mathbf{k}/2$ is given by

$$\int \sigma f^{(2)}(\mathbf{c}_1,\mathbf{r}_1,\mathbf{c}_2,\mathbf{r}_2)(\mathbf{q}\cdot\mathbf{k})(\mathbf{k}\cdot\mathbf{n})d\mathbf{k}\,d\mathbf{c}_1\,d\mathbf{c}_2, \qquad (A1)$$

where $f^{(2)}(\cdot)$ is the two-particle distribution function which is defined so that $f^{(2)}(\mathbf{c}_1,\mathbf{r}_1,\mathbf{c}_2,\mathbf{r}_2)\,d\mathbf{c}_1\,d\mathbf{c}_2\,d\mathbf{r}_1\,d\mathbf{r}_2$ is the number of pairs of particles such that the particle i is located in an area element $d\mathbf{r}_1$ about $\mathbf{r}_1$ with its velocity in the interval $d\mathbf{c}_1$ about $\mathbf{c}_1$ while particle j is located in an area element $d\mathbf{r}_2$ about $\mathbf{r}_2$ with its velocity in the interval $d\mathbf{c}_2$ about $\mathbf{c}_2$. To progress further, we have to invoke the assumption of molecular chaos and hence the expected number of collisions is

$$\int \sigma g(\mathbf{r}_1,\mathbf{r}_2)f^{(1)}(\mathbf{c}_1,\mathbf{r}_1;\mathbf{u}(\mathbf{r}_1))f^{(1)}(\mathbf{c}_2,\mathbf{r}_2;\mathbf{u}(\mathbf{r}_2))(\mathbf{q}\cdot\mathbf{k})$$
$$\times(\mathbf{k}\cdot\mathbf{n})d\mathbf{k}\,d\mathbf{c}_1\,d\mathbf{c}_2, \qquad (A2)$$

where $g(\mathbf{r}_1,\mathbf{r}_2)$ is the pair-distribution function. For the steady uniform shear flow, $g(\mathbf{r}_1,\mathbf{r}_2)$ is calculated from the relation[35,36,58]

$$g(\mathbf{r}_1,\mathbf{r}_2)=\frac{2g_c(\nu)}{n^2}\int_{\mathbf{q}\cdot\mathbf{k}>0}f^{(1)}(\mathbf{c}_1,\mathbf{r}_1;\mathbf{u}(\mathbf{r}_1))$$
$$\times f^{(1)}(\mathbf{c}_2,\mathbf{r}_2;\mathbf{u}(\mathbf{r}_2))d\mathbf{c}_1\,d\mathbf{c}_2, \qquad (A3)$$

where $g_c(\nu)$ is the *contact* value of the pair-distribution function and $\mathbf{q}\cdot\mathbf{k}>0$ implies that the integration be carried out for impending collisions.

As a first approximation, the single particle velocity distribution function $f^{(1)}(\mathbf{c}_1,\mathbf{r}_1;\mathbf{u}(\mathbf{r}_1))$ is assumed to have the Maxwellian-form

$$f^{(1)}(\mathbf{c}_1,\mathbf{r}_1;\mathbf{u}(\mathbf{r}_1))=\left(\frac{nm}{\pi k_{\mathrm B}T}\right)\exp\left[-\frac{m(\mathbf{c}_1-\mathbf{u}(\mathbf{r}_1))^2}{2k_{\mathrm B}T}\right], \qquad (A4)$$

where T is the granular temperature (fluctuating kinetic energy) and $k_{\mathrm B}$ the usual Boltzmann constant. Now transforming the particle velocities ($\mathbf{c}_1$, $\mathbf{c}_2$) to their center-of-mass and relative velocities, Eq. (A3) can be integrated to arrive at the following explicit expression for the pair-distribution function:[36]

$$g(\mathbf{r}_1,\mathbf{r}_2)=g_c(\nu)\mathrm{erfc}\left[\frac{2\mathbf{k}\cdot\mathbf{u}(\mathbf{r}_2)}{(2k_{\mathrm B}T)^{1/2}}\right], \qquad (A5)$$

where $\mathrm{erfc}(\cdot)$ is the complementary error function. Using the above expression for the pair-distribution function and transforming in terms of polar coordinates (r,θ), the integral for the normalized collision angle distribution yields[37]

$$C(\theta)=\mathcal{A}(T)\left[\exp\left(-\frac{\sin^2\theta\cos^2\theta}{2T}\right)\right.$$
$$\left.-\frac{g(\theta)\sin\theta\cos\theta}{\sqrt{T}}\right]g(\theta), \qquad (A6)$$

where $g(\theta)$ is the angular pair-distribution function given by

$$g(\theta)\equiv\frac{g(\mathbf{r}_1,\mathbf{r}_2)}{g_c(\nu)}=\mathrm{erfc}\left[\frac{\sin\theta\cos\theta}{\sqrt{2T}}\right], \qquad (A7)$$

and $\mathcal{A}(T)$ is a normalization constant.

For the uniform shear flow, an expression for the granular temperature, can be obtained from the energy balance equation, by equating the energy production due to shear-work with the energy loss due to collisions:

$$\mu\left(\frac{du}{dy}\right)^2=\mathcal{D}\Rightarrow T=f_\mu(\nu)/f_{\mathcal{D}}(\nu,e), \qquad (A8)$$

where $\mu=\rho_p\sigma f_\mu(\nu)\sqrt{T}$ is the shear viscosity and $\mathcal{D}=(\rho_p/\sigma)f_{\mathcal{D}}(\nu,e)T^{3/2}$ the collisional dissipation rate, with

$$f_\mu(\nu)=\frac{\sqrt{\pi}\nu}{8}\left[\frac{1}{\nu g_c(\nu)}+2+\nu g_c(\nu)\left(1+\frac{8}{\pi}\right)\right],$$

$$f_{\mathcal{D}}(\nu,e)=\frac{4}{\sqrt{\pi}}(1-e^2)\nu^2 g_c(\nu).$$

Substituting this expression for T, the normalized collision distribution function becomes

$$C(\theta;\nu,e)=\mathcal{A}(T)\left[\exp\left(-\frac{f_{\mathcal{D}}(\nu,e)\sin^2\theta\cos^2\theta}{2f_\mu(\nu)}\right)\right.$$
$$\left.-g(\theta)\sin\theta\cos\theta\sqrt{\frac{f_{\mathcal{D}}(\nu,e)}{f_\mu(\nu)}}\right]g(\theta), \qquad (A9)$$

and the angular pair-distribution function,

$$g(\theta;\nu,e)=\mathrm{erfc}\left[\sin\theta\cos\theta\sqrt{\frac{f_{\mathcal{D}}(\nu,e)}{2f_\mu(\nu)}}\right]. \qquad (A10)$$

It is clear that the angular dependence of $C(\theta;\nu,e)$ is modified by both the inelastic dissipation and the density.

[1] H.J. Herrmann, J.-P. Hovi, and S. Luding, *Physics of Dry Granular Media*, NATO ASI Series E 350 (Kluwer Academic, Dordrecht, 1998).

[2] T. Pöschel and S. Luding, *Granular Gases*, Lecture Notes in Physics 764 (Springer-Verlag, Berlin, 2001).

[3] C.S. Campbell, "Rapid granular flows," Annu. Rev. Fluid Mech. **22**, 57 (1990).

[4] I. Goldhirsch and N. Sela, "Origin of normal stress differences in rapid granular flows," Phys. Rev. E **54**, 4458 (1996).

[5] N. Sela and I. Goldhirsch, "Hydrodynamic equations for rapid flows of smooth inelastic spheres to Burnett order," J. Fluid Mech. **361**, 41 (1998).

[6] J.D. Goddard, "Dissipative materials as models of thixotropy and plasticity," J. Non-Newtonian Fluid Mech. **14**, 141 (1984).

[7] R.B. Bird, R.C. Armstrong, and O. Hassager, *Dynamics of Polymeric Liquids* (Wiley, London, 1977).

[8] J.D. Goddard, "Polymer fluid mechanics," Adv. Appl. Mech. **19**, 143 (1977).

[9] J.D. Goddard and M. Alam, "Shear-flow and material instabilities in particulate suspensions and granular media," Part. Sci. Technol. **17**, 69 (1999).

[10] P. Coussot, Q.D. Nguyen, H.T. Huynh, and D. Bonn, "Avalanche behavior in yield stress fluids," Phys. Rev. Lett. **88**, 175501 (2002).

[11] M.A. Hopkins and M.Y. Louge, "Inelastic microstructure in rapid granular flows of smooth disks," Phys. Fluids A **3**, 47 (1991).

[12] I. Goldhirsch and D. Zanetti, "Clustering instability in dissipative gases," Phys. Rev. Lett. **70**, 1619 (1993).

[13] S. Luding and H.J. Herrmann, "Cluster growth in freely cooling granular media," Chaos **9**, 673 (1999).

[14] S.B. Savage, "Instability of unbounded uniform granular shear flow," J. Fluid Mech. **241**, 109 (1992).

[15] M. Alam and P.R. Nott, "Stability of plane Couette flow of a granular material," J. Fluid Mech. **377**, 99 (1998).

[16] J.T. Jenkins and R.W. Richman, "Plane simple shear of smooth inelastic circular disks: the anisotropy of the second moment in the dilute and dense limit," J. Fluid Mech. **192**, 313 (1988).

[17] J.D. Goddard and A.K. Didwania, "Computations of dilatancy and yield surfaces for assemblies of rigid frictional spheres," Q. J. Mech. Appl. Math. **39**, 145 (1997).

[18] M. Reiner, "A mathematical theory of dilatancy," Am. J. Math. **67**, 350 (1945).

[19] C.S. Campbell and A. Gong, "The stress tensor in a two-dimensional granular shear flow," J. Fluid Mech. **164**, 107 (1986).

[20] O.R. Walton and R.L. Braun, "Viscosity, granular-temperature, and stress calculations for shearing assemblies of inelastic, frictional disks," J. Rheol. **30**, 949 (1986).

[21] M.P. Allen and D.J. Tildesley, *Computer Simulations of Liquids* (Clarendon, Oxford, 1989).

[22] A.W. Lees and S.F. Edwards, "The computer study of transport processes under extreme conditions," J. Phys. C **5**, 1921 (1972).

[23] M. Alam and S. Luding, "How good is the equipartition assumption for the transport properties of a granular mixture?" Granular Matter **4**, 139 (2002).

[24] M. Alam and S. Luding, "Rheology of bidisperse granular mixtures via event-driven simulations," J. Fluid Mech. **476**, 69 (2003).

[25] E.D. Liss and B.J. Glasser, "The influence of clusters on the stress in a sheared granular material," Powder Technol. **116**, 116 (2001).

[26] S. Luding, "Global equation of state of two-dimensional hard sphere systems," Phys. Rev. E **63**, 042201 (2001).

[27] S. Luding and O. Strauss, "The equation of state of polydisperse granular gases," in *Granular Gases*, Lecture Notes in Physics 564, edited by T. Pöschel and S. Luding (Springer-Verlag, Berlin, 2001).

[28] M.W. Richman, "The source of second moment in dilute granular flows of highly inelastic spheres," J. Rheol. **33**, 1293 (1989).

[29] A. Santos, J.M. Montanero, J. Dufty, and J.J. Brey, "Kinetic model for the hard-sphere fluid and solid," Phys. Rev. E **57**, 1644 (1998).

[30] R.L. Fosdick and K.R. Rajagopal, "Anomalous features in the model of second order fluids," Arch. Ration. Mech. Anal. **70**, 145 (1979).

[31] J.F. Brady and M. Vivic, "Normal stresses in colloidal dispersions," J. Rheol. **39**, 545 (1995).

[32] D.R. Foss and J.F. Brady, "Structure, diffusion and rheology of Brownian suspensions by Stokesian dynamics simulations," J. Fluid Mech. **407**, 167 (2000).

[33] S. Luding, "Structures and non-equilibrium dynamics in granular media," C. R. Acad. Sci., Ser. IV: Phys. Astrophys. **3**, 153 (2002).

[34] L.V. Woodcock and C.A. Angel, "Diffusivity of the hard-sphere model in the region of fluid metastability," Phys. Rev. Lett. **47**, 1129 (1981).

[35] J.G. Kirkwood, F.P. Buff, and M.S. Green, "The statistical mechanical theory of transport processes," J. Chem. Phys. **17**, 988 (1949).

[36] S.B. Savage and D.J. Jeffrey, "The stress tensor in a granular flow at high shear rates," J. Fluid Mech. **110**, 255 (1981).

[37] C.S. Campbell and C.E. Brennen, "Computer simulation of granular shear flows," J. Fluid Mech. **151**, 167 (1985).

[38] J.T. Jenkins and E. Askari, "Boundary conditions for rapid granular flows: phase interfaces," J. Fluid Mech. **223**, 497 (1991).

[39] S. McNamara and W.R. Young, "Inelastic collapse in two dimensions," Phys. Rev. E **50**, R28 (1994).

[40] S. Luding and S. McNamara, "How to handle the inelastic collapse of a dissipative hard particle gas with the TC model?" Granular Matter **1**, 113 (1998).

[41] S. Luding and A. Goldshtein, "Hydrodynamic theory for dissipative hard spheres with multi-particle interactions," Granular Matter (in press).

[42] P.R. Nott, M. Alam, K. Agrawal, R. Jackson, and S. Sundaresan, "The effect of boundaries on the plane Couette flow of granular materials: A bifurcation analysis," J. Fluid Mech. **397**, 203 (1999).

[43] M.-L. Tan, "Microstructures and macrostructures in rapid granular flows," Ph.D. thesis, Princeton University, 1995.

[44] C.S. Campbell, "Granular shear flows at the elastic limit," J. Fluid Mech. **465**, 261 (2002).

[45] J.F. Lutsko, "Molecular chaos, pair correlation, and shear-induced ordering of hard spheres," Phys. Rev. Lett. **77**, 2225 (1996).

[46] J. Erpenbeck, "Shear viscosity of the hard sphere fluid via nonequilibrium molecular dynamics," Phys. Rev. Lett. **52**, 1333 (1984).

[47] D.J. Evans and G.P. Morriss, "Shear thickening and turbulence in simple fluids," Phys. Rev. Lett. **56**, 2172 (1986).

[48] S.B. Savage and S. Sayed, "Stresses developed by dry cohesionless granular materials in an annular shear cell," J. Fluid Mech. **142**, 391 (1984).

[49] H. Grad, "On the kinetic theory of rarefied gases," Commun. Pure Appl. Math. **2**, 331 (1949).

[50] J.T. Jenkins and M.W. Richman, "Grad's 13-moment system for a dense gas of inelastic spheres," Arch. Ration. Mech. Anal. **87**, 355 (1985).

[51] S. Jin and M. Slemrod, "Regularization of the Burnett equations for rapid granular flows via relaxation," Physica D **150**, 207 (2001).

[52] D.Z. Zhang and R.M. Rauenzahn, "A viscoelastic model for dense granular flows," J. Rheol. **41**, 1275 (1997).

[53] D.Z. Zhang and R.M. Rauenzahn, "Stress relaxation in dense and slow granular flows," J. Rheol. **44**, 1019 (2000).

[54] E. Ikenberry and C. Truesdell, "On the pressures and flux of energy in a gas according to Maxwell's kinetic theory," J. Ration. Mech. Anal. **5**, 1 (1956).

[55] I. Müller, "On the frame dependence of stress and heat flux," Arch. Ration. Mech. Anal. **45**, 241 (1972).

[56] M. Lee, J. Dufty, J. Montanero, A. Santos, and J.F. Lutsko, "Long wavelength instability for uniform shear flow," Phys. Rev. Lett. **76**, 2702 (1996).

[57] R. Soto, J. Piasecki, and M. Mareschal, "Precollisional velocity correlations in a hard-disk fluid with dissipative collisions," Phys. Rev. E **64**, 031306 (2001).

[58] S. Hess, "Structure of liquids and solids in nonequilibrium," J. Phys. C **46**, 191 (1985).